
Adding 3D Geometry Control to Diffusion Models

Wufei Ma^{1*} Qihao Liu^{1*} Jiahao Wang^{1*} Angtian Wang¹
Yaoyao Liu^{1†} Adam Kortylewski^{2,3} Alan Yuille¹

¹Johns Hopkins University ²University of Freiburg ³Max Planck Institute for Informatics

Abstract

Diffusion models have emerged as a powerful method of generative modeling across a range of fields, capable of producing stunning photo-realistic images from natural language descriptions. However, these models lack explicit control over the 3D structure of the objects in the generated images. In this paper, we propose a novel method that incorporates 3D geometry control into diffusion models, making them generate even more realistic and diverse images. To achieve this, our method exploits ControlNet [1], which extends diffusion models by using visual prompts in addition to text prompts. We generate images of 3D objects taken from a 3D shape repository (e.g., ShapeNet [2] and Objaverse [3]), render them from a variety of poses and viewing directions, compute the edge maps of the rendered images, and use these edge maps as visual prompts to generate realistic images. With explicit 3D geometry control, we can easily change the 3D structures of the objects in the generated images and obtain ground-truth 3D annotations automatically. This allows us to use the generated images to improve a lot of vision tasks, e.g., classification and 3D pose estimation, in both in-distribution (ID) and out-of-distribution (OOD) settings. We demonstrate the effectiveness of our method through extensive experiments on ImageNet-50, ImageNet-R, PASCAL3D+, ObjectNet3D, and OOD-CV datasets. The results show that our method significantly outperforms existing methods across multiple benchmarks (e.g., 4.6 percentage points on ImageNet-50 using ViT [4] and 3.5 percentage points on PASCAL3D+ and ObjectNet3D using NeMo [5]).

1 Introduction

Understanding the underlying 3D world of 2D images is essential to numerous computer vision tasks. The utilization of 3D modeling opens up the possibility of addressing a significant portion of the variability inherent in natural images, which could potentially enhance the overall understanding and interpretation of images [6, 7]. For example, 3D-aware models show high robustness and generalization ability under occlusion or environmental changes [5, 8]. However, it is expensive and time-consuming to obtain ground-truth 3D annotations for 2D images. This training data shortage becomes a main obstacle to training large-scale 3D-aware models.

Recently, diffusion models [9] have shown impressive performance in generating photo-realistic images, which can be used to solve the training data shortage. These models allow us to produce high-quality images from various conditional inputs, e.g., natural language descriptions, segmentation maps, and keypoints [1]. This facilitates generative data augmentation, e.g., He et al. [10] use diffusion models to augment ImageNet [11] and significantly improve the classification results.

Despite their success, diffusion models still lack explicit control over the underlying 3D world during the generation process. As a result, they still face two challenges that hinder their use in augmenting

*Equal contribution.

†Corresponding author: Yaoyao Liu (yliu538@jhu.edu)

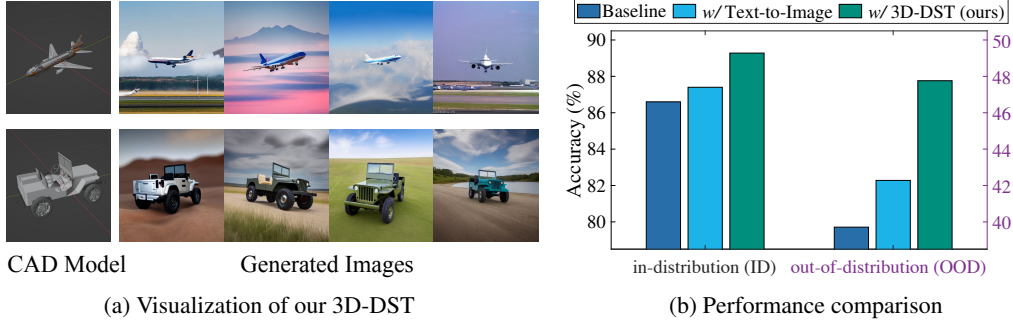


Figure 1: (a) **Visualization of our 3D-DST.** Our proposed solution, 3D-DST, leverages both 3D visual prompts and large language model (LLM) text prompts to generate diverse images from a CAD model. The use of 3D visual prompts enables explicit control over the 3D structure of the object within the generated images, such as varying 3D poses and distances. On the other hand, LLM text prompts facilitate the automatic generation of images with diverse backgrounds, weather conditions, and colors. (b) **Performance comparison.** Our 3D-DST model can be utilized to generate data to enhance both in-distribution (ID) and out-of-distribution (OOD) performance. The baseline is ResNet-50. “Text-to-Image” denotes using diffusion models that do not incorporate 3D control to augment the data [10]. The experiments are conducted on ImageNet-50.

data for 3D tasks. The first challenge is the inability to control the 3D properties of the object in the generated images, such as pose and distance. The second challenge is the difficulty in obtaining ground-truth 3D annotations of objects automatically.

To tackle the above challenges, we propose a novel framework, 3D-controlled diffusion style transfer (3D-DST), which enables us to incorporate knowledge about 3D geometry structures. To achieve this, our method exploits ControlNet [1], which extends diffusion models by using visual prompts in addition to text prompts. We generate images of 3D objects taken from a 3D shape repository (e.g., ShapeNet [2] and Objaverse [3]), render them from a variety of viewing directions and distances, compute the edge maps of the rendered images, and use these edge maps as visual prompts to generate realistic images. With explicit 3D geometry control, we can easily change the 3D structures of the objects in the generated images and obtain corresponding 3D annotations automatically.

To enhance the diversity of the generated images, we apply the following strategies. Firstly, we vary the viewing directions in which the 3D objects are rendered. This generates a wide range of edge maps and allows us to produce multiple distinct images for each 3D object. Secondly, we introduce a novel prompting technique to improve diversity further. We input essential information about the 3D objects into large language models (LLM) [12] to obtain reasonable descriptions, such as background and color. Then, we use these descriptions as the text prompts for diffusion models. This not only enables us to make the most of the vast potential of the diffusion models but also helps us to avoid generating images that are too similar. These two strategies allow us to generate diverse images that can be used to improve the out-of-distribution (OOD) robustness of AI models. As shown in Figure 1, our 3D-DST effectively generates images with a wide range of viewpoints, distances, colors, and backgrounds. These generated images have proven valuable in enhancing performance across both in-distribution (ID) and OOD scenarios.

We conduct extensive experiments to show the effectiveness of our method. Firstly, we show that our method can be directly used as a data augmentation method for classification. For example, our method improves the ImageNet-50 accuracy by 4.6 percentage points on ViT [4]. Secondly, we demonstrate that our method is able to boost the performance of 3D-aware models. With automatically produced 3D annotations, pre-training on our generated images can improve the 3D pose estimation benchmark, PASCAL3D+ [13], by 3.9 and 2.4 percentage points in ID and OOD settings, respectively (accuracy @ $\pi/18$).

To summarise, we make **three contributions**. (1) We design a novel pipeline that allows us to add 3D conditional control to diffusion models. This allows us to obtain 3D annotations of the generated images easily. (2) We propose novel techniques to enhance the diversity of the generated images, e.g., creating reasonable prompts with LLM. (3) We conduct comprehensive experiments

to demonstrate the efficacy of our pipeline in creating a high-quality, photo-realistic dataset that includes 3D annotations on a large scale. This dataset has the potential to enhance a wide range of vision-related tasks, such as classification and 3D pose estimation, particularly in challenging scenarios involving occlusions and out-of-distribution samples.

2 Related Work

Synthetic data augmentation. Synthetic data has gained significant attention in generating labeled data for vision tasks that require extensive annotations [1, 14–16]. The utilization of synthetic data augmentation methods can be categorized into two groups: 2D-based and 3D-based methods. 2D-based methods employ recent generative models like GANs and diffusion models to create photo-realistic images, effectively expanding datasets for tasks such as semantic image segmentation [17–19], optical flow estimation [20, 21], human motion understanding [22, 23], and other dense prediction tasks. Despite their effectiveness, these methods lack 3D structures, making it challenging to acquire 3D annotations for the generated images. On the other hand, 3D-based methods leverage simulation environments with physically realistic engines to render 3D models and generate images [24, 25]. However, the generated images’ diversity is limited as they heavily rely on the existing textures of the 3D models. In our work, we investigate the integration of 3D structure control into diffusion models. This approach allows us to generate diverse images using the appearance produced by diffusion models while obtaining 3D annotations through the 3D structure conditions.

Diffusion models operate by incrementally degrading the data through introducing Gaussian noise gradually, and subsequently learn to restore the data by reversing this noise infusion process [9, 26, 27]. They have shown remarkable success in generating high-resolution photo-realistic images from various conditional inputs, e.g., natural language descriptions, segmentation maps, and keypoints [1, 9, 28]. Recently, text-to-image diffusion models have also been used to augment training data. He et al. [10] demonstrate that the use of a synthetic dataset can notably enhance the accuracy of CIFAR-100 classification. Trabucco et al. [29] investigate various strategies for augmenting individual images with the help of a pre-trained diffusion model, showcasing considerable enhancements in few-shot learning scenarios. Azizi et al. [30] present evidence that the usage of class names as text prompts can guide the diffusion models to generate images that subsequently improve performance in ImageNet classification tasks.

Despite their advancements, diffusion models still face limitations in explicitly controlling the 3D structure of the images they generate. Our research contributes to overcoming this challenge by integrating 3D geometry conditional inputs into diffusion models. This enhancement empowers us with precise control over the 3D structure of the object within the produced image, and facilitates effortless acquisition of 3D annotations, such as 3D pose key points.

Large language models (LLM). The field of natural language processing has witnessed a transformative shift in recent years, spurred by the advent of large language models such as GPT-3 [31], PaLM [32], and LLaMA [12]. These large language models have showcased remarkable proficiency in zero-shot and few-shot tasks, as well as more intricate assignments like mathematical problem-solving and commonsense reasoning. Their impressive performance can be attributed to the extensive corpora they are trained on and the intensive computational resources dedicated to their training. In our study, we utilize LLaMA [12] to enhance the quality of text prompts. By automatically generating descriptive prompts pertaining to backgrounds, color, and weather conditions, we successfully improve the diversity of our generated images.

3 Methodology

As illustrated in Figure 2, our proposed 3D-DST enhances diffusion models [9] by incorporating both 3D visual prompts and diverse text prompts. In Section 3.1, we describe how existing diffusion models [1, 14] incorporate 2D visual and simple text conditions for generative data augmentation. In Section 3.2, we introduce how to produce visual prompts based on 3D geometry conditions by graphics-based rendering. In Section 3.3, we show how to create text prompts with LLM [12] to enhance the diversity. Algorithm 1 summarizes how to generate images with 3D annotations using our 3D-DST.

3.1 Background: Diffusion Models with Text and 2D Visual Prompts

Diffusion models [1, 9, 14] achieve great success in conditional image generation using text and 2D visual prompts. In the following, we first introduce the original diffusion models without conditional inputs. Then, we show how to add text prompts by augmenting the underlying U-Net backbone of the diffusion models with a cross-attention mechanism [14]. Moreover, we elaborate on how to integrate 2D visual prompts using the ControlNet architecture [1].

Diffusion model pipeline. Diffusion models [9, 14] learn to generate images by learning a sequence of denoising U-Nets. Starting from a random noise z_T , the denoising process is as follows,

$$z_{t-1} = \epsilon(z_t, t), \quad t = T \dots 1, \quad (1)$$

where $\epsilon(z_t, t)$ denotes the denoising U-Nets. z_{t-1} is a denoise version of the input z_t . In the final step, z_0 is input to a pre-trained decoder \mathcal{D} to get the generated image I_{final} , i.e., $I_{\text{final}} = \mathcal{D}(z_0)$.

While diffusion models have achieved significant success in image synthesis, the original version [9] does not inherently support conditional control. In the following, we show how to add text and 2D visual controls to the diffusion models.

Adding text prompts via cross-attention. Existing works [1, 14, 30] effectively employ text prompts, such as class names or keywords, as guidance for diffusion models, enabling them to generate images that adhere to specific content requirements. To achieve this, they incorporate text prompts into diffusion models using the cross-attention mechanism [33], following [14]. First, they pre-process the text prompts \mathcal{T} with a pre-trained text encoder θ . Then, they map the prompts to the intermediate layers of the U-Net ϵ via cross-attention layers:

$$\phi_i = \text{softmax} \left(\frac{QK^M}{\sqrt{|\phi_{i-1}|}} \right) \cdot V, \quad Q = W_Q^{(i)} \cdot \phi_{i-1}, \quad K = W_K^{(i)} \cdot \theta(\mathcal{T}), \quad V = W_V^{(i)} \cdot \theta(\mathcal{T}), \quad (2)$$

where ϕ_i denotes the i -th layer intermediate representation of the U-Net ϵ , and $\phi_i = z_t$. $W_Q^{(i)}$, $W_K^{(i)}$, and $W_V^{(i)}$ are learnable projection matrices. M is a hyperparameter of the cross-attention.

Adding 2D visual prompts via ControlNet. To integrate 3D visual prompts into diffusion models, the ControlNet architecture [1] is utilized. It enables the incorporation of 3D visual prompts without retraining the entire diffusion model.

During Step t of the denoising process, the 2D visual prompts \mathcal{E}_{2D} are added to the latent variable z_t , and the resulting sum is inputted into the ControlNet. Then, the outputs of the ControlNet will be integrated into the denoising U-Net ϵ following [1], i.e.,

$$z_{t-1} = \epsilon(z_t, \mathcal{T}, \text{ControlNet}(z_t + \mathcal{E}_{2D})). \quad (3)$$

Limitations of existing methods. Although current approaches have achieved notable success, they continue to encounter the following challenges. Firstly, these methods lack 3D geometry control, making it arduous to explicitly modify the 3D structure of objects within generated images and acquire pertinent 3D annotations, such as 3D pose key points. Secondly, existing methods frequently depend on simple text prompts to guide the image generation process when augmenting datasets with diffusion models [30]. Consequently, the diversity of produced images remains restricted.

In order to address these challenges, in the following, we demonstrate the generation of 3D visual prompts through graphics-based rendering and augment the text prompts with LLaMA, effectively enhancing the diversity of the generated images.

3.2 3D Visual Prompts by Graphics-based Rendering

In order to effectively integrate 3D geometry control into diffusion models, it is essential to ensure that the visual prompts meet the following two specific requirements.

Firstly, the visual prompts must encompass sufficient information to depict the 3D geometry structure of the objects accurately. Without this information, it would be challenging to achieve explicit control over the 3D structure of the objects (e.g., shape and pose) in the generated images, consequently hindering the generation of corresponding 3D annotations.

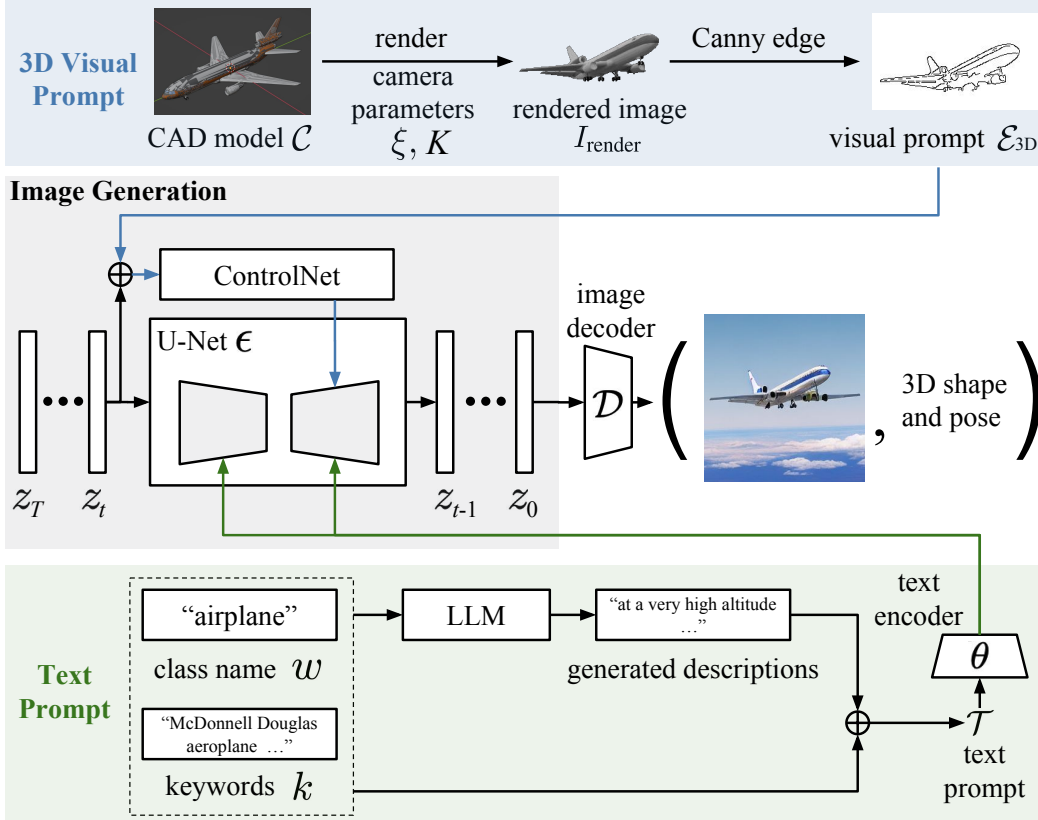


Figure 2: Our 3D-DST comprises three essential steps. (1) **3D visual prompt generation.** We generate images of 3D objects taken from a 3D shape repository (e.g., ShapeNet [2] and Objaverse [3]), render them from a variety of viewpoints and distances, compute the edge maps of the rendered images, and use these edge maps as 3D visual prompts. (2) **Text prompt generation.** Our approach involves combining the class names of objects with the associated tags or keywords of the CAD models. This combined information forms the initial text prompts. Then, we enhance these prompts by incorporating the descriptions generated by LLM [12]. (3) **Image generation.** We generate photo-realistic images with 3D visual and text prompts using Stable Diffusion [14] and ControlNet [1].

Secondly, the visual prompts should be compact and concise, enabling diffusion models to comprehend and effectively process them. Utilizing overly complex visual prompts, such as the vertices and meshes of a CAD model, would prove impractical and unfeasible for the diffusion models to handle efficiently. Therefore, it is crucial to strike a balance and employ visual prompts that are both informative and manageable within the diffusion model framework.

To satisfy the aforementioned requirements, our proposed approach involves generating visual prompts through graphics-based rendering. We leverage CAD models obtained from a 3D shape repository such as ShapeNet [2] and Objaverse [3]. Then, we render the CAD models from diverse viewpoints and distances, compute edge maps based on the rendered images and utilize these edge maps as visual prompts. This approach enables us to encapsulate the necessary information regarding the 3D geometry structure of the objects. The rendered images provide essential details such as the viewing directions and distances, facilitating explicit control over the 3D structure during the generation of images. By extracting edge maps, we create compact visual prompts that are suitable for integration within diffusion models.

In the following, we will elaborate on the detailed steps.

Graphics-based rendering. We render CAD models with various viewing directions and distances and then obtain the rendered sketch images. Given a CAD model \mathcal{C} , we generate the rendered sketch images I_{render} as follows,

$$I_{\text{render}} = R(\mathcal{C}, \xi, K), \quad (4)$$

where R denotes an off-the-shelf renderer, i.e., [34], K is the camera intrinsic matrix, ξ represents a camera extrinsic matrix computed from a randomized viewing direction and distance follows a predefined distribution. In practice, we use the Perspective camera with focal length $f = 35\text{mm}$ to render the images. Complex backgrounds are not necessary here because the rendered sketch images are used to extract edge maps.

Edge map computation. Next, we extract edge maps from the rendered sketch images. The primary objective of this process is to enhance the compactness and conciseness of the rendered images while preserving the underlying 3D geometry structure. To achieve this, we apply classical edge detection methods, e.g., Canny edge [35]. Given a rendered sketch images I_{render} , we obtain the edge map \mathcal{E}_{3D} as follows,

$$\mathcal{E}_{3D} = \text{CannyEdge}(I_{\text{render}}). \quad (5)$$

Then, we use \mathcal{E}_{3D} as the 3D visual prompt for the CAD model \mathcal{C} , replacing \mathcal{E}_{2D} in Eq. 3.

3.3 Diverse Text Prompts by LLM

Text prompts play a crucial role in guiding diffusion models to generate diverse images [14]. However, current data augmentation methods based on diffusion models often rely on overly simplistic text prompts to guide the image generation process. For example, [30] utilizes class names directly as text prompts, while [1] employs a default prompt such as ‘‘a high-quality, detailed, and professional image.’’ These simplistic approaches fail to fully harness the rich appearance information stored within diffusion models.

To address the aforementioned issue, we present a novel strategy for text prompt generation. Our approach involves combining the class names of objects with the associated tags or keywords of the CAD models. This combined information forms the initial text prompts. Then, we enhance these prompts by incorporating the descriptions generated by LLM [12]. The final text prompts \mathcal{T} of a CAD model \mathcal{C} are created as follows,

$$\mathcal{T} = \{t, w, k, \text{LLM}(t, w, k)\}, \quad (6)$$

where t represents a prompt template, such as ‘‘a photo of \dots ’’. w corresponds to the one-word class name of the CAD model \mathcal{C} , while k denotes the tags or keywords associated with \mathcal{C} in the 3D shape repository (e.g., ShapeNet [2] and Objaverse [3]). LLM [12] is a large language model capable of generating rich and coherent descriptions (e.g., backgrounds, colors) when provided with the initial text prompts (t, w, k) .

3.4 Algorithm

Algorithm 1 provides a comprehensive summary of generating images with 3D annotations using our 3D-DST. The steps are detailed below. (1) Lines 4-7 delineate the pre-processing involved in each iteration, which encompasses loading a new CAD model from the 3D shape repository and initializing the camera parameters. (2) Lines 9-12 illustrate the generation of 3D visual prompts, which involves rendering the images, generating 3D annotations, and computing the edge maps. (3) Lines 13-14 depict the process of generating diverse text prompts with the aid of LLM [12] (4) Lines 15-19 detail the image generation process, utilizing diffusion models.

4 Experiments

In this section, we demonstrate how our 3D-DST synthetic data can be used to boost the performance of deep learning models for both 2D recognition task, i.e., image classification, and 3D vision tasks,

Algorithm 1 Generating images using our 3D-DST

```

1: Input: 3D shape repository  $\{\mathcal{C}, w, k\}$ .
2: Output: Images with 3D annotations  $\{I_{\text{final}}, y_{3D}\}$ .
3: for iterations do
4:   Get a CAD model  $\mathcal{C}$  from the 3D shape repository;
5:   Load the class name  $w$  and keyword  $k$  of  $\mathcal{C}$ ;
6:   Load the camera intrinsic matrix  $K$ ;
7:   Generate randomized camera extrinsic matrices  $\{\xi\}$ ;
8:   for different camera extrinsic matrix  $\xi$  do
9:     // 3D visual prompt generation
10:    Render sketch image  $I_{\text{render}}$  using  $\xi$  and  $K$  by Eq. 4;
11:    Produce 3D annotations  $y_{3D}$  of  $I_{\text{render}}$ ;
12:    Compute edge map  $\mathcal{E}_{3D}$  using Canny Edge by Eq. 5 ;
13:    // Text prompt generation
14:    Create text prompts  $\mathcal{T}$  using  $w$  and  $k$  by Eq. 6;
15:    // Image generation
16:    Initialize a random noise  $z_T$ ;
17:    for  $t$  in  $T, \dots, 1$  do
18:      | Denoise  $z_t$  to  $z_{t-1}$  using  $\mathcal{T}$  and  $\mathcal{E}_{3D}$  by Eq. 3;
19:      | Generate images  $I_{\text{final}} = \mathcal{D}(z_0)$ .
20:    Collect the generated dataset  $\{I_{\text{final}}, y_{3D}\}$ .

```

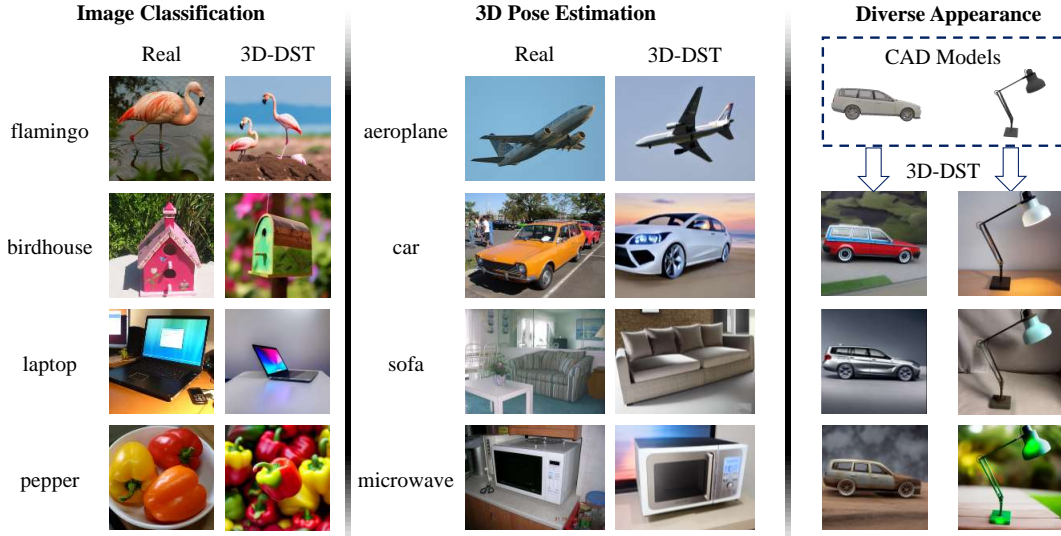


Figure 3: **Left and center:** Visualizations of 3D-DST synthetic data for image classification and 3D pose estimation. **Right:** objects with various appearance can be generated from only a limited number of CAD models by conditioning on diverse textual prompts.

i.e., 3D pose estimation on standard benchmarks as well as on out-of-distribution data. We first describe how to build the 3D-DST synthetic datasets in Section 4.1. Then we present quantitative results on ID benchmarks and OOD data for image classification in Section 4.2 and for 3D pose estimation in Section 4.3.

4.1 3D-DST Synthetic data

A key component of our 3D-DST framework is a collection of CAD models for each class or category. Despite the abundant CAD models available on the Internet, we demonstrate in Figure 3 that we could use as few as 30 CAD models for each category and generate unlimited number of objects with variations in shape and appearance with the help of diverse textual prompts and the large capacity of the pre-trained Stable Diffusion model [14]. This largely simplifies the amount of work to develop our synthetic dataset and makes our approach extendable to a large scale.

In this work, we collect around 30 CAD models from the ShapeNet dataset [2] or the Objaverse dataset [3] for each object class we consider. Then we run our 3D-DST framework and generate 2,500 images for each class. We experiment with different dataset sizes, i.e., 1,500 and 2,000 in the supplementary materials. We visualize a few sample images for classes from ImageNet [36] or PASCAL3D+ [13] in Figure 3 and more visualizations are available in the supplementary materials.

4.2 Robust Image Classification

Datasets. We consider ImageNet-50 [36] and ImageNet-R [37] for quantitative evaluation on ID data and OOD data, respectively. ImageNet [36] is a large visual database containing 14,197,122 real images hand-annotated with 21,841 synsets (classes). In this paper, we use a subset of 50 classes to speed up the experiments. ImageNet-R has renditions of 200 ImageNet classes resulting in 30,000 images, and the renditions include art, cartoons, graphics, origami, paintings, patterns, plastic objects, plush objects, sculptures, sketches, tattoos, toys, video games, etc. Thus, ImageNet-R is out of the distribution of images in ImageNet. We evaluate various representative classification models on 50 categories from ImageNet and 19 categories from ImageNet-R, which are the categories that overlap with our dataset.

Models. To show how synthetic data help improve the classification results, we use ResNet [38] and Vision Transformer (ViT) [4] as the classifiers. For ResNet, we use ResNet-50, which is a 50-layer convolution neural network architecture. ViT is a transformer-based architecture, and we use ViT-S,

Methods	in-distribution (ID)		out-of-distribution (OOD)	
	ResNet-50	ViT-S	ResNet-50	ViT-S
ImageNet-50	86.60	84.72	39.71	37.19
ImageNet-50 + Text2Img [10]	87.40	85.68	42.28	36.31
	(↑0.80)	(↑0.96)	(↑2.57)	(↓0.88)
ImageNet-50 + 3D-DST (ours)	89.28	89.36	47.76	39.68
	(↑2.68)	(↑4.64)	(↑8.05)	(↑2.49)

Table 1: Top-1 accuracy of image classification on ImageNet-50 (ID) and ImageNet-R (OOD). We evaluate ResNet-50 and ViT-S. We compare the performances when models are (1) trained purely on ImageNet-50, (2) pretrained on Text2Img [10] data, which does not have 3D control, and then finetuned on ImageNet, (3) pretrained on 3D-DST data, and finetuned on ImageNet-50. Experiments show that our 3D-DST data can help boost the classification accuracy of both models on both ID and OOD cases by a large margin.

which has a comparable number of parameters as ResNet-50. We follow the implementation from the DeiT [39] codebase for all models.

Training and testing. For in-distribution (ID) classification, we compare the models in three different settings. The first setting is to train models purely on ImageNet-50 for 600 epochs. The second setting is to pretrain the models on the images generated by a text-to-image (Text2Img) model without 3D control [10] for 300 epochs, and finetune on ImageNet-50 for 300 epochs. The third setting is to pretrain the models on our 3D-DST synthetic data first for 300 epochs, and finetune on ImageNet-50 for 300 epochs. We test all of them on ImageNet-50. For the out-of-domain (OOD) classification, we follow similar training settings, but only train on the 19 classes that overlap with the categories in the ImageNet-R dataset, and we test the models on the 19 classes in the ImageNet-R dataset. During training, the input image size is 224×224 , the batch size is set to 512, and we use AdamW [40] as the optimizer. The initial learning rate is $1e - 4$ and we use a cosine scheduler for learning rate decay. We use Rand-Augment [41], random erasing [42], Mixup [43] and Cutmix [44] for data augmentation, following the setting in [39]. More details about computational resources are in the appendix.

Evaluation. Following previous works [4, 38, 39, 45], we evaluate the models using the Top-1 classification accuracy on ImageNet-50 (ID) and ImageNet-R (OOD).

Quantitative results on ImageNet-50 (ID) and ImageNet-R (OOD). As shown in Table 1, we can see that our 3D-DST synthetic data can consistently improve all the models in both ID case and OOD case by a large margin. On ImageNet, with the help of 3D-DST data, the Top-1 accuracy of ResNet-50 and ViT-S are increased by 2.68 and 4.64 percentage points, respectively. As a comparison, the Text2Img [10] dataset can only improve the classification accuracy by a small margin, i.e., 0.80 and 0.96 percentage points for ResNet-50 and ViT-S, respectively. For the OOD test, Text2Img [10] dataset can only improve the performance of ResNet-50, and the accuracy drops for ViT-S, while the 3D-DST data can consistently improve both models. For ResNet-50 and ViT-S, the accuracy is improved by 8.05 and 2.49 percentage points, which indicates the great potential of using the 3D-DST data to improve model robustness.

4.3 Robust Category-Level 3D Pose Estimation

Datasets. We consider PASCAL3D+, ObjectNet3D, and OOD-CV. The PASCAL3D+ dataset [13] contains 11, 045 training images and 10, 812 validation images of 12 man-made object categories with category and object pose annotations. The OOD-CV dataset [46, 47] includes OOD examples from 10 categories of PASCAL3D+ and is a benchmark to evaluate out-of-distribution robustness to individual nuisance factors, including pose, shape, appearance, context, and weather. The ObjectNet3D dataset is another 3D pose estimation benchmark that contains 100 categories with 17, 101 training samples and 19, 604 testing samples. Following previous works [5, 46], we evaluate pose estimation models on 10 categories from PASCAL3D+ and a subset of ObjectNet3D with 10 categories.

Methods	P3D+ & ObjectNet3D (ID)		OOD-CV (OOD)	
	Acc@ $\pi/6$	Acc@ $\pi/18$	Acc@ $\pi/6$	Acc@ $\pi/18$
ResNet50	82.33	52.60	50.38	23.38
ResNet50 w/ AugMix [49]	82.72 ($\uparrow 0.39$)	53.89 ($\uparrow 1.29$)	51.77 ($\uparrow 1.39$)	24.57 ($\uparrow 1.19$)
ResNet50 w/ 3D-DST (ours)	84.22 ($\uparrow 1.89$)	56.52 ($\uparrow 3.92$)	52.75 ($\uparrow 2.37$)	25.70 ($\uparrow 2.32$)
NeMo [5]	82.23	57.12	55.31	26.57
NeMo w/ 3D-DST (ours)	85.70 ($\uparrow 3.47$)	62.51 ($\uparrow 5.39$)	58.81 ($\uparrow 3.50$)	26.44 ($\downarrow 0.13$)

Table 2: Robust 3D pose estimation on PASCAL3D+ [13], ObjectNet3D [50], and OOD-CV [46]. We experiment with a classification-based pose estimation method, ResNet50, and a 3D compositional model, NeMo [5]. Experimental results demonstrate that our DST synthetic data can effectively improve 3D pose estimation performance on both ID and OOD benchmarks.

Models. To demonstrate how synthetic data can be used to improve the state-of-the-art performance on category-level 3D pose estimation, we adopt the state-of-the-art method, NeMo [5], which estimates 3D poses with analysis-by-synthesis using neural mesh models. Moreover, we also consider classification-based methods that formulate pose estimation as a classification problem. We follow the implementation from [48] that extends a ResNet-50 model with a pose classification head.

Evaluation. Following previous works [5, 48], we measure the 3D pose prediction with the pose estimation error between the predicted rotation matrix and the ground truth rotation matrix $\Delta(\mathbf{R}_{\text{pred}}, \mathbf{R}_{\text{gt}}) = \frac{\|\log(\mathbf{R}_{\text{pred}}^T \mathbf{R}_{\text{gt}})\|_F}{\sqrt{2}}$. We report results under thresholds $\frac{\pi}{6}$ and $\frac{\pi}{18}$, following [5, 48].

Quantitative results on PASCAL3D+ and ObjectNet3D. We consider two training setups for 3D pose estimation: (i) directly train the models on real data from PASCAL3D+ and ObjectNet3D dataset; and (ii) pretrain the models on 3D-DST and then finetune on real data. We evaluate various pose estimation methods on the validation set of the PASCAL3D+ and ObjectNet, and the results are reported in Table 2. As we can see, our synthetic data can effectively improve the 3D pose estimation results by 1.89 and 3.47 percentage points with a threshold of $\frac{\pi}{6}$ and by 3.92 and 5.39 percentage points for $\frac{\pi}{18}$. As a comparison, we also train pose estimation methods with a strong data augmentation method, AugMix [49], that mixes augmented images and enforces consistent embeddings of the augmented images. When evaluated on in-distribution validation data from PASCAL3D+ and ObjectNet3D, AugMix brings limited improvements compared to our 3D-DST.

Robust 3D pose estimation on OOD-CV. From the right column of Table 2, our 3D-DST data can effectively improve the model’s performance on out-of-distribution data, e.g., with a gap of 2.37 and 3.50 percentage points for $\frac{\pi}{6}$. This shows that our approach with 3D-DST can introduce diverse data not present in the training data and improve the robustness of models to various domain shifts.

5 Conclusion

In this work, we introduce a novel framework, 3D-DST, which incorporates 3D geometry control into diffusion models. This empowers us with explicit control over the 3D structure of the objects in the generated images. As a result, we can conveniently acquire ground-truth 3D annotations for the produced 2D images. To boost the diversity of the images, we adjust 3D poses and distances and employ LLM for creating dynamic text prompts. Our empirical results reveal that the images generated by our method can significantly enhance performance across a range of vision tasks, including classification and 3D pose estimation, in both ID and OOD settings.

Limitations and broader impact. We analyze the limitations and potential negative societal impact in the following two aspects. (1) Technical assumptions. We build our 3D-DST framework based on a series of technical assumptions, which might not directly hold for all real-world applications. When applying our method to mission-critical problems, particular care is required when modeling the system. (2) Privacy issues. Generating data from the diffusion model may have data privacy issues. This calls for future research that explicitly controls the generated contents.

References

- [1] Lvmin Zhang and Maneesh Agrawala. Adding conditional control to text-to-image diffusion models. *arXiv preprint arXiv:2302.05543*, 2023. [1](#), [2](#), [3](#), [4](#), [5](#), [6](#)
- [2] Angel X Chang, Thomas Funkhouser, Leonidas Guibas, Pat Hanrahan, Qixing Huang, Zimo Li, Silvio Savarese, Manolis Savva, Shuran Song, Hao Su, et al. Shapenet: An information-rich 3d model repository. *arXiv preprint arXiv:1512.03012*, 2015. [1](#), [2](#), [5](#), [6](#), [7](#), [15](#)
- [3] Matt Deitke, Dustin Schwenk, Jordi Salvador, Luca Weihs, Oscar Michel, Eli VanderBilt, Ludwig Schmidt, Kiana Ehsani, Aniruddha Kembhavi, and Ali Farhadi. Objaverse: A universe of annotated 3d objects. *arXiv preprint arXiv:2212.08051*, 2022. [1](#), [2](#), [5](#), [6](#), [7](#), [15](#)
- [4] Alexey Dosovitskiy, Lucas Beyer, Alexander Kolesnikov, Dirk Weissenborn, Xiaohua Zhai, Thomas Unterthiner, Mostafa Dehghani, Matthias Minderer, Georg Heigold, Sylvain Gelly, et al. An image is worth 16x16 words: Transformers for image recognition at scale. *arXiv preprint arXiv:2010.11929*, 2020. [1](#), [2](#), [7](#), [8](#), [13](#)
- [5] Angtian Wang, Shengxiao Mei, Alan L. Yuille, and Adam Kortylewski. Neural view synthesis and matching for semi-supervised few-shot learning of 3d pose. In *NeurIPS*, pages 7207–7219, 2021. [1](#), [8](#), [9](#), [13](#)
- [6] Shangzhe Wu, Christian Rupprecht, and Andrea Vedaldi. Unsupervised learning of probably symmetric deformable 3d objects from images in the wild. In *CVPR*, pages 1–10, 2020. [1](#)
- [7] Animesh Karnewar, Andrea Vedaldi, David Novotny, and Niloy Mitra. Holodiffusion: Training a 3d diffusion model using 2d images. In *CVPR*, 2023. [1](#)
- [8] Qihao Liu, Yi Zhang, Song Bai, and Alan L. Yuille. Explicit occlusion reasoning for multi-person 3d human pose estimation. In *ECCV*, pages 497–517, 2022. [1](#)
- [9] Jonathan Ho, Ajay Jain, and Pieter Abbeel. Denoising diffusion probabilistic models. In Hugo Larochelle, Marc’Aurelio Ranzato, Raia Hadsell, Maria-Florina Balcan, and Hsuan-Tien Lin, editors, *NeurIPS*, 2020. [1](#), [3](#), [4](#)
- [10] Ruifei He, Shuyang Sun, Xin Yu, Chuhui Xue, Wenqing Zhang, Philip Torr, Song Bai, and Xiaojuan Qi. Is synthetic data from generative models ready for image recognition? In *ICLR*, 2023. [1](#), [2](#), [3](#), [8](#)
- [11] Jia Deng, Wei Dong, Richard Socher, Li-Jia Li, Kai Li, and Li Fei-Fei. Imagenet: A large-scale hierarchical image database. In *CVPR*, pages 248–255, 2009. [1](#)
- [12] Hugo Touvron, Thibaut Lavril, Gautier Izacard, Xavier Martinet, Marie-Anne Lachaux, Timothée Lacroix, Baptiste Rozière, Naman Goyal, Eric Hambro, Faisal Azhar, et al. Llama: Open and efficient foundation language models. *arXiv preprint arXiv:2302.13971*, 2023. [2](#), [3](#), [5](#), [6](#)
- [13] Yu Xiang, Roozbeh Mottaghi, and Silvio Savarese. Beyond pascal: A benchmark for 3d object detection in the wild. In *WACV*, pages 75–82, 2014. [2](#), [7](#), [8](#), [9](#), [15](#)
- [14] Robin Rombach, Andreas Blattmann, Dominik Lorenz, Patrick Esser, and Björn Ommer. High-resolution image synthesis with latent diffusion models. In *CVPR*, pages 10684–10695, 2022. [3](#), [4](#), [5](#), [6](#), [7](#)
- [15] Yaoyao Liu, Qianru Sun, Xiangnan He, An-An Liu, Yuting Su, and Tat-Seng Chua. Generating face images with attributes for free. *TNNLS*, 32(6):2733–2743, 2021.
- [16] Yaoyao Liu, Yuting Su, An-An Liu, Bernt Schiele, and Qianru Sun. Mnemonics training: Multi-class incremental learning without forgetting. In *CVPR*, pages 12242–12251, 2020. [3](#)
- [17] Dmitry Baranchuk, Andrey Voynov, Ivan Rubachev, Valentin Khrukov, and Artem Babenko. Label-efficient semantic segmentation with diffusion models. In *ICLR*, 2022. [3](#)
- [18] Daiqing Li, Huan Ling, Seung Wook Kim, Karsten Kreis, Sanja Fidler, and Antonio Torralba. Bigdatasetgan: Synthesizing imagenet with pixel-wise annotations. In *CVPR*, pages 21330–21340, 2022.

- [19] Nontawat Tritrong, Pitchaporn Rewatbowornwong, and Supasorn Suwajanakorn. Repurposing gans for one-shot semantic part segmentation. In *CVPR*, pages 4475–4485, 2021. 3
- [20] Alexey Dosovitskiy, Philipp Fischer, Eddy Ilg, Philip Hausser, Caner Hazirbas, Vladimir Golkov, Patrick Van Der Smagt, Daniel Cremers, and Thomas Brox. Flownet: Learning optical flow with convolutional networks. In *ICCV*, pages 2758–2766, 2015. 3
- [21] Deqing Sun, Daniel Vlasic, Charles Herrmann, Varun Jampani, Michael Krainin, Huiwen Chang, Ramin Zabih, William T Freeman, and Ce Liu. Autoflow: Learning a better training set for optical flow. In *CVPR*, pages 10093–10102, 2021. 3
- [22] Xi Guo, Wei Wu, Dongliang Wang, Jing Su, Haisheng Su, Weihao Gan, Jian Huang, and Qin Yang. Learning video representations of human motion from synthetic data. In *CVPR*, pages 20197–20207, 2022. 3
- [23] Gul Varol, Javier Romero, Xavier Martin, Naureen Mahmood, Michael J Black, Ivan Laptev, and Cordelia Schmid. Learning from synthetic humans. In *CVPR*, pages 109–117, 2017. 3
- [24] Klaus Greff, Francois Belletti, Lucas Beyer, Carl Doersch, Yilun Du, Daniel Duckworth, David J Fleet, Dan Gnanapragasam, Florian Golemo, Charles Herrmann, et al. Kubric: A scalable dataset generator. In *CVPR*, pages 3749–3761, 2022. 3
- [25] Jia Zheng, Junfei Zhang, Jing Li, Rui Tang, Shenghua Gao, and Zihan Zhou. Structured3d: A large photo-realistic dataset for structured 3d modeling. In *ECCV*, pages 519–535, 2020. 3
- [26] Uriel Singer, Adam Polyak, Thomas Hayes, Xi Yin, Jie An, Songyang Zhang, Qiyuan Hu, Harry Yang, Oron Ashual, Oran Gafni, et al. Make-a-video: Text-to-video generation without text-video data. *arXiv preprint arXiv:2209.14792*, 2022. 3
- [27] Ruben Villegas, Mohammad Babaeizadeh, Pieter-Jan Kindermans, Hernan Moraldo, Han Zhang, Mohammad Taghi Saffar, Santiago Castro, Julius Kunze, and Dumitru Erhan. Phenaki: Variable length video generation from open domain textual description. *arXiv preprint arXiv:2210.02399*, 2022. 3
- [28] Jonathan Ho, Chitwan Saharia, William Chan, David J Fleet, Mohammad Norouzi, and Tim Salimans. Cascaded diffusion models for high fidelity image generation. *JMLR*, 23(47):1–33, 2022. 3
- [29] Brandon Trabucco, Kyle Doherty, Max Gurinas, and Ruslan Salakhutdinov. Effective data augmentation with diffusion models. *arXiv preprint arXiv:2302.07944*, 2023. 3
- [30] Shekoofeh Azizi, Simon Kornblith, Chitwan Saharia, Mohammad Norouzi, and David J Fleet. Synthetic data from diffusion models improves imagenet classification. *arXiv preprint arXiv:2304.08466*, 2023. 3, 4, 6
- [31] Tom B. Brown, Benjamin Mann, Nick Ryder, Melanie Subbiah, Jared Kaplan, Prafulla Dhariwal, Arvind Neelakantan, and Pranav Shyam. Language models are few-shot learners. In *NeurIPS*, 2020. 3
- [32] Aakanksha Chowdhery, Sharan Narang, Jacob Devlin, Maarten Bosma, Gaurav Mishra, Adam Roberts, and Paul Barham. Palm: Scaling language modeling with pathways. *arXiv preprint arXiv:2204.02311*, 2022. 3
- [33] Ashish Vaswani, Noam Shazeer, Niki Parmar, Jakob Uszkoreit, Llion Jones, Aidan N Gomez, Lukasz Kaiser, and Illia Polosukhin. Attention is all you need. *NeurIPS*, pages 5998–6008, 2017. 4
- [34] Blender Online Community. *Blender - a 3D modelling and rendering package*. Blender Foundation, Stichting Blender Foundation, Amsterdam, 2018. 6
- [35] John Canny. A computational approach to edge detection. *TPAMI*, 8(6):679–698, 1986. 6
- [36] Olga Russakovsky, Jia Deng, Hao Su, Jonathan Krause, Sanjeev Satheesh, Sean Ma, Zhiheng Huang, Andrej Karpathy, Aditya Khosla, Michael Bernstein, Alexander C. Berg, and Li Fei-Fei. ImageNet Large Scale Visual Recognition Challenge. *IJCV*, 115(3):211–252, 2015. 7

- [37] Dan Hendrycks, Steven Basart, Norman Mu, Saurav Kadavath, Frank Wang, Evan Dorundo, Rahul Desai, Tyler Zhu, Samyak Parajuli, Mike Guo, et al. The many faces of robustness: A critical analysis of out-of-distribution generalization. In *ICCV*, pages 8340–8349, 2021. 7
- [38] Kaiming He, Xiangyu Zhang, Shaoqing Ren, and Jian Sun. Deep residual learning for image recognition. In *CVPR*, pages 770–778, 2016. 7, 8, 13
- [39] Hugo Touvron, Matthieu Cord, Matthijs Douze, Francisco Massa, Alexandre Sablayrolles, and Hervé Jégou. Training data-efficient image transformers & distillation through attention. In *International conference on machine learning*, pages 10347–10357. PMLR, 2021. 8, 13
- [40] Ilya Loshchilov and Frank Hutter. Decoupled weight decay regularization. *arXiv preprint arXiv:1711.05101*, 2017. 8, 13
- [41] Ekin D Cubuk, Barret Zoph, Jonathon Shlens, and Quoc V Le. Randaugment: Practical automated data augmentation with a reduced search space. In *CVPR Workshops*, pages 702–703, 2020. 8, 13
- [42] Zhun Zhong, Liang Zheng, Guoliang Kang, Shaozi Li, and Yi Yang. Random erasing data augmentation. In *AAAI*, 2020. 8, 13
- [43] Hongyi Zhang, Moustapha Cisse, Yann N Dauphin, and David Lopez-Paz. mixup: Beyond empirical risk minimization. *arXiv preprint arXiv:1710.09412*, 2017. 8, 13
- [44] Sangdoon Yun, Dongyoon Han, Seong Joon Oh, Sanghyuk Chun, Junsuk Choe, and Youngjoon Yoo. Cutmix: Regularization strategy to train strong classifiers with localizable features. In *ICCV*, pages 6023–6032, 2019. 8, 13
- [45] Yaoyao Liu, Yingying Li, Bernt Schiele, and Qianru Sun. Online hyperparameter optimization for class-incremental learning. In *AAAI*, 2023. 8
- [46] Bingchen Zhao, Shaozuo Yu, Wufei Ma, Mingxin Yu, Shenxiao Mei, Angtian Wang, Ju He, Alan Yuille, and Adam Kortylewski. Ood-cv: A benchmark for robustness to out-of-distribution shifts of individual nuisances in natural images. In *ECCV*, pages 163–180, 2022. 8, 9
- [47] Bingchen Zhao, Jiahao Wang, Wufei Ma, Artur Jesslen, Siwei Yang, Shaozuo Yu, Oliver Zendel, Christian Theobalt, Alan Yuille, and Adam Kortylewski. Ood-cv-v2: An extended benchmark for robustness to out-of-distribution shifts of individual nuisances in natural images. *arXiv preprint arXiv:2304.10266*, 2023. 8
- [48] Xingyi Zhou, Arjun Karapur, Linjie Luo, and Qixing Huang. Starmap for category-agnostic keypoint and viewpoint estimation. In *ECCV*, pages 318–334, 2018. 9, 13
- [49] Dan Hendrycks, Norman Mu, Ekin Dogus Cubuk, Barret Zoph, Justin Gilmer, and Balaji Lakshminarayanan. Augmix: A simple method to improve robustness and uncertainty under data shift. In *ICLR*, 2020. 9
- [50] Yu Xiang, Wonhui Kim, Wei Chen, Jingwei Ji, Christopher Choy, Hao Su, Roozbeh Mottaghi, Leonidas Guibas, and Silvio Savarese. Objectnet3d: A large scale database for 3d object recognition. In *ECCV*, pages 160–176, 2016. 9, 15

Supplementary Materials

A Additional Results

Qualitative examples. We visualize some sample images from our 3D-DST dataset in Figure S1. To demonstrate how diverse prompts from LLM can help to generate diverse outputs in textures and backgrounds, we show some qualitative comparisons in Figure S2 between 3D-DST data with and without diverse prompts from LLM (when not using LLM, we only use the class names from ImageNet and descriptions from the CAD models as simple prompts).

3D-DST without using LLM prompts. To evaluate the effectiveness of using LLM to generate prompts, we conduct quantitative experiments of training ResNet-50 [38] and ViT-S [4] on 3D-DST data with and without using LLM prompts, respectively. We finetune and test all of them on ImageNet-50. The quantitative results are shown in Table S1. The results show that using LLM prompts can achieve better results compared with only using simple prompts. One possible reason is that using LLM can help generate more diverse data as shown in Figure S2.

Different dataset sizes. We compare the classification accuracy when using 3D-DST with different numbers of images. We train the models on 3D-DST data with 1500, 2000, and 2500 images per class, respectively. The results in Table S2 show that using 3D-DST with only 1500 per class can already improve the accuracy by 2 percentage points on average, and using more data can further improve the classification performance of all the models. Note that we can easily scale up 3D-DST dataset by generating synthetic images with ground truth using our pipeline, without the need to manually collect and annotate images.

Error bar. It would be too computationally expensive to report the error bars for all the experiments. However, we compute the error bar for a main experiment in the paper, i.e., the top-1 classification accuracy of the three models trained on ImageNet-50 + 3D-DST, by only changing the random seeds and keeping all the other settings the same. The standard deviations of the classification accuracy of ResNet-50, and ViT-S are 0.12% and 0.06%, respectively.

B Model Training

Image classification. We follow the implementation from the DeiT [39] codebase for all models. During training, the input image size is 224×224 , the batch size is set to 512, and we use AdamW [40] as the optimizer. The initial learning rate is $1e - 4$ and we use a cosine scheduler for learning rate decay. We use Rand-Augment [41], random erasing [42], Mixup [43] and Cutmix [44] for data augmentation. We use two NVIDIA Quadro RTX 8000 GPUs for each training. For other settings, we refer to [39].

3D pose estimation. For the classification-based model, ResNet50, we use the released implementation from [48] and trained the model for 90 epochs with a learning rate of 0.01. For NeMo, we adopt the publicly released code [5] and trained the NeMo models for 800 epochs on both the synthetic and real data. Each NeMo model is trained on four NVIDIA RTX A5000 for 10 hours.

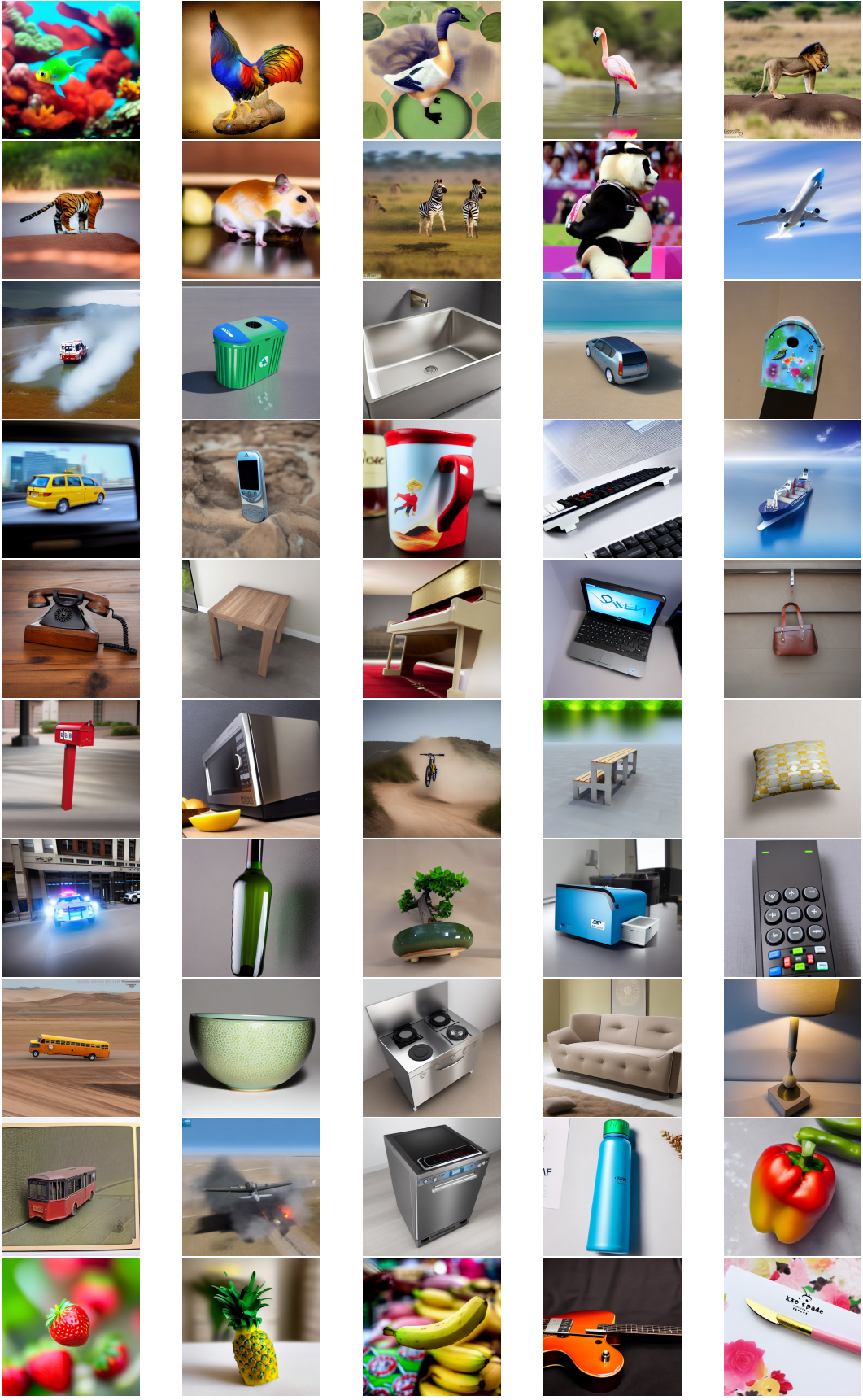


Figure S1: Samples images from our 3D-DST dataset.



Figure S2: Qualitative comparison between 3D-DST data generated with diverse prompts with LLM and simple prompts crafted by hand.

Methods	ResNet-50	ViT-S
ImageNet-50	86.60	84.72
ImageNet-50 + 3D-DST w/o LLM prompts	88.96	88.72
	($\uparrow 2.36$)	($\uparrow 4.00$)
ImageNet-50 + 3D-DST (ours)	89.28	89.36
	($\uparrow 2.68$)	($\uparrow 4.64$)

Table S1: Top-1 accuracy of image classification on ImageNet-50. We evaluate 3 representative models, ResNet-50 and ViT-S. We compare the performances when models are (1) trained purely on ImageNet-50, (2) pretrained on 3D-DST data generated without using LLM prompts (only use simple prompts like class names and keywords from the CAD model descriptions), and then finetuned on ImageNet, (3) pretrained on 3D-DST data, and finetuned on ImageNet-50. Experiments show that our 3D-DST data can help boost the classification accuracy of both models by a large margin, and using LLM prompts can help achieve better results.

C More Details about Generating 3D-DST Synthetic Data

The 50 classes we used in the classification experiment are listed in Table S3. We collect 30 CAD models for each class from the ShapeNet dataset [2] and the Objaverse dataset [3], and 2,500 images were rendered for each class. We sample the object viewpoint with a uniform distribution over the azimuth angle and Gaussian distributions over the elevation and theta angles. The viewpoint sampling rules are detailed in Table S4. For pose estimation, we estimate the mean and variance of the object viewpoints from the training data of PASCAL3D+ [13] and ObjectNet3D [50] and sample from the fitted Gaussian distributions.

Methods	ResNet-50	ViT-S
ImageNet-50	86.60	84.72
ImageNet-50 + 3D-DST 1500	88.16	87.12
ImageNet-50 + 3D-DST 2000	88.72	88.28
ImageNet-50 + 3D-DST 2500	89.28	89.36

Table S2: Comparison of the effects of different dataset sizes when 3D-DST contains 1500, 2000, and 2500 synthetic images per class, respectively. We evaluate Top-1 accuracy of image classification on ImageNet-50 for ResNet-50 and ViT-S. Experiments show that only using 3D-DST with 1500 per class can already improve the accuracy a lot, and using more data can further improve the classification performance of all the models.

synset	class name
<u>n01443537</u>	goldfish, Carassius auratus
n01514668	cock
n01855672	goose
<u>n02007558</u>	flamingo
<u>n02129165</u>	lion, king of beasts, Panthera leo
<u>n02129604</u>	tiger, Panthera tigris
n02342885	hamster
<u>n02391049</u>	zebra
<u>n02510455</u>	giant panda, panda, panda bear, coon bear, Ailuropoda melanoleuca
n02676566	acoustic guitar
n02690373	airliner
<u>n02701002</u>	ambulance
n02747177	ashcan, trash can, garbage can, wastebin, ash bin, ash-bin, ashbin, dustbin, trash barrel, trash bin
<u>n02808440</u>	bathtub, bathing tub, bath, tub
n02814533	beach wagon, station wagon, wagon, estate car, beach waggon, station waggon, waggon
<u>n02843684</u>	birdhouse
n02930766	cab, hack, taxi, taxicab
<u>n02992529</u>	cellular telephone, cellular phone, cellphone, cell, mobile phone
n03063599	coffee mug
n03085013	computer keyboard, keypad
n03095699	container ship, containership, container vessel
n03187595	dial telephone, dial phone
n03201208	dining table, board
<u>n03452741</u>	grand piano, grand
n03642806	laptop, laptop computer
n03658185	letter opener, paper knife, paperknife
n03709823	mailbag, postbag
<u>n03710193</u>	mailbox, letter box
n03761084	microwave, microwave oven
n03792782	mountain bike, all-terrain bike, off-roader
n03891251	park bench
n03938244	pillow
n03977966	police van, police wagon, paddy wagon, patrol wagon, wagon, black Maria
n03983396	pop bottle, soda bottle
n03991062	pot, flowerpot
n04004767	printer
n04074963	remote control, remote
<u>n04146614</u>	school bus
n04263257	soup bowl
n04330267	stove
n04344873	studio couch, day bed
n04380533	table lamp
n04487081	trolleybus, trolley coach, trackless trolley
<u>n04552348</u>	warplane, military plane
n04554684	washer, automatic washer, washing machine
n04557648	water bottle
<u>n07720875</u>	bell pepper
<u>n07745940</u>	strawberry
<u>n07753275</u>	pineapple, ananas
<u>n07753592</u>	banana

Table S3: The related ImageNet synsets and class names of the 50 classes used in 3D-DST classification. The 19 synsets with underlines are the classes overlapping with ImageNet-R that are used in OOD experiments.

Azimuth	Elevation	Theta	Classes
all	all	$\mathcal{N}(0, \pi/18)$	airliner, beach wagon, cab, coffee mug, dining table, piano bicycle, pillow, police van, pot, school bus, warplane, bottle bench, birdhouse, ambulance, trolleybus
front	all	$\mathcal{N}(0, \pi/18)$	cellular phone, laptop, mailbox, microwave, remote control washer, bag
all	top	$\mathcal{N}(0, \pi/18)$	keyboard, table lamp, trash can, bathtub, couch, soup bowl
front	top	$\mathcal{N}(0, \pi/18)$	printer, stove

Table S4: Viewpoint sampling rules for 3D-DST generated for image classification.